Journal of Materials Chemistry C

Accepted Manuscript

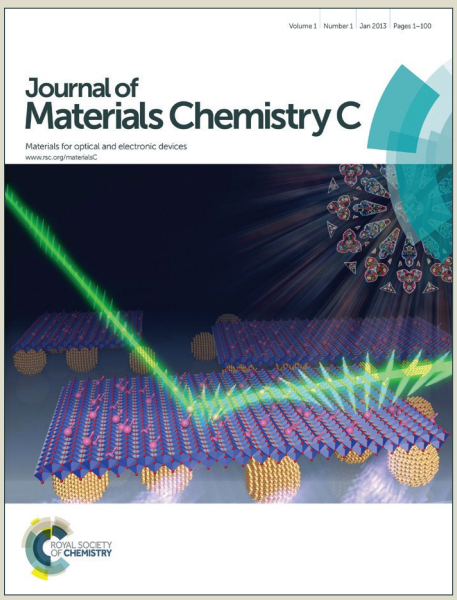

ROYAL SOCIETY OF CHEMISTRY

www.rsc.org/materialsC

Cite this: DOI: 10.1039/c0xx00000x

www.rsc.org/xxxxxx

ARTICLE TYPE

Simultaneous Harvesting of Triplet Excitons in OLEDs by both Guest and Host Materials with Intramolecular Charge-transfer Feature *via* Triplet-Triplet Annihilation†

Xujun Zheng,[a‡] Qiming Peng,[b‡] Jie Lin,[c‡] Yi Wang,[a] Jie Zhou,[a] Yan Jiao,[a] Yuefeng Bai,[d] Yan Huang,[a] Feng Li,*[b] Xingyuan Liu,*[c] Xuemei Pu,[a] Zhiyun Lu*[a]

Received (in XXX, XXX) Xth XXXXXXXXX 20XX, Accepted Xth XXXXXXXXX 20XX
DOI: 10.1039/b000000x

A red naphthalimide derivative with intramolecular charge-transfer (ICT) feature, namely (*E*)-2-(4-(*t*-butyl)phenyl)-6-(2-(6-(diphenylamino)naphthalen-2-yl)vinyl)-1*H*-benzo[*de*]isoquinoline-1,3(2*H*)-dione (**NA-TNA**), was designed and synthesized. Photophysical and magneto-electroluminescence (MEL) characterization results revealed that **NA-TNA** could harvest triplet excitons *via* triplet-triplet annihilation (TTA) process in organic light-emitting diodes (OLEDs) due to the presence of a lower-lying triplet excited state with $^3\pi\pi^*$ character. Consequently, using **NA-TNA** as guest compound and CzPhONI, another ICT-featured naphthalimide derivative with triplet fusion delayed fluorescence (TFDF) character as host material, a high-performance orange OLED with 6 wt% **NA-TNA** doped CzPhONI film as the emitting layer was acquired. The maximum current efficiency (LE_{max}), brightness (L_{max}), and external quantum yield (EQE_{max}) of this OLED is 7.73 cd/A, 31940 cd/m^2 and 5.83%, respectively, while the theoretical EQE_{max} of this device should not exceed 3.34%. On the contrary, the reference device with **NA-TNA** doping level of 1.4 wt% showed much inferior performance, with LE_{max}, L_{max}, and EQE_{max} of 3.19 cd/A, 24900 cd/m^2 and 2.49%, respectively. The high performance of the 6 wt% **NA-TNA** doped device was attributed to the efficient harvesting of triplet excitons by both the guest and host materials.

Introduction

In the past two decades, OLEDs have been regarded as the "third generation of flat panel display" and the "next generation of lighting technology", and have attracted much attention in both scientific and industrial communities.[1–4] According to electroluminescence (EL) mechanism, OLEDs could be classified into two main categories, namely fluorescent (FOLEDs) and phosphorescent ones (PhOLEDs). Although high reliability has been achieved in FOLEDs, the maximum internal quantum efficiency (IQE_{max}) of FOLEDs is generally limited to 25% according to spin statistics.[5] While for PhOLEDs, although high IQE_{max} of 100% could be achieved,[6] their disadvantage lies in the relatively high cost of the rare metal complexes.[4,7]

Recently, FOLEDs capable of harvesting both singlet and triplet excitons have aroused great research interest due to their combined high efficiency and low cost.[3,4,8] Nowadays, three possible mechanisms have been reported for such FOLEDs, namely thermally-activated delayed fluorescence (TADF), hybridized local and charge-transfer excited state (HLCT), and triplet-fusion delayed fluorescence (TFDF). For TADF-OLEDs, although their potential IQE_{max} could reach 100%,[7,9–11] the conflict between small singlet-triplet energy gap (ΔE_{ST}) and high radiative rate within TADF luminogens makes it difficult to design high-performance TADF materials rationally.[4,11] While for HLCT materials,[4,12-14] although high photoluminescent (PL) efficiency could be achieved, these compounds should disobey the Kasha's rule, so that the internal conversion from T_n to T_m states (m<n) could be blocked effectively.[14,15] Therefore, the rational molecular design of HLCT materials is still a great challenge.[3] However, for OLEDs based on TFDF materials, their IQE_{max} could reach 62.5% if triplet excitons could be up-converted efficiently into singlet ones through triplet-triplet annihilation (TTA) process.[8,16-24] More importantly, the harvesting of triplet excitons could be realized not only by the non-doped emitters[21,22] and doping guests at relative high doping levels,[17,23] but also by the host compounds with TFDF character.[24] Because the prerequisite for TFDF materials is $2E_T \geq E_S$, which could be fulfilled by many conjugated systems whose S_1 and T_1 states are both of $\pi\pi^*$ character,[25-29] the rational molecular design of TFDF materials should be easier than that of TADF and HLCT compounds.

Currently, most of the research works related to TFDF-OLEDs are focused on the elucidation of the role TTA process plays in the enhancement of EL efficiency;[19-20] while the TFDF compounds used are generally limited to those with $\pi\pi^*$ character.[25-29] However, our recent study has revealed that ICT-featured compounds could also act as promising TFDF materials if they possess a lowest triplet excited state with $^3\pi\pi^*$ character.[30] Because most of the lower-bandgap fluorophores like orange and red ones are D-π-A compounds with ICT feature,[31-33] and the harvesting of

triplet excitons could be actualized by TFDF-guests if their doping levels are relatively high,[17,23] the development of novel lower-bandgap ICT-TFDF guest fluorophores with alleviated concentration quenching may give access to high-performance OLEDs with desirable batch-to-batch reproducibility for massive production. Moreover, if the host compound also displays TFDF character, triplet excitons might be utilized not only by the TFDF guest dopant, but also by the TFDF-host compound through TTA process followed by efficient energy transfer (ET) from host to guest materials.[30] Yet to the best of our knowledge, so far no reports could be found using TFDF-charactered hosts and guests to harvest triplet excitons simultaneously in OLEDs.

Inspired by our recent discovery that the ICT compound CzPhONI (structure shown in Fig. 1) is a promising TFDF-host material for high-performance OLED,[30] and fluorophores with good structural similarity could form efficient ET pair,[34] herein, we report the design and synthesis of an ICT-featured red D-π-A fluorophore **NA-TNA** (Fig. 1), in which diphenylamine, vinylnaphthalene and 1,8-naphthalimide acts as electron donor (D), π-bridge and electron acceptor (A), respectively. As both CzPhONI and **NA-TNA** are 1,8-naphthalimide derivatives, they could form an efficient host/guest ET pair; and the presence of a bulky diphenylamine D segment in **NA-TNA** could endow it with suppressed intermolecular interactions. In addition, similar to CzPhONI, **NA-TNA** also shows TFDF property. Using **NA-TNA** as guest and CzPhONI as host materials, a 6 wt% **NA-TNA** doped OLED with LE_{max} of 7.73 cd/A, L_{max} of 31940 cd/m^2, and EQE_{max} of 5.83% was achieved, and the high performance of this device was attributed to the concurrent harvesting of triplet excitons by the host and guest materials *via* TTA process.

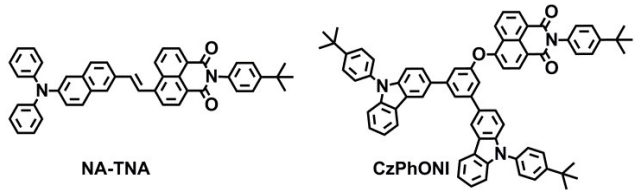

Fig. 1 Molecular structure of **NA-TNA** and CzPhONI.

Experimental section

General Information

All the commercially available chemicals were directly used without further purification unless otherwise stated. All the solvents were of analytical grade and were freshly distilled prior to use. ^{1}H NMR and ^{13}C NMR spectra were measured using a Bruker Avance AV II-400 MHz spectrometer, and the chemical shifts were recorded in units of ppm with TMS as the internal standard. Coupling constants (*J*) were reported in Hertz. FT-IR spectra were recorded on a Perkin-Elmer 2000 infrared spectrometer with KBr pellets under an ambient atmosphere. High resolution MS spectra were measured with a Q-TOF Premier ESI mass spectrometer (Micromass, Manchester, UK). Thermogravimetric analysis (TGA) and differential scanning calorimetry (DSC) were performed on TGA Q500 and DSC Q100 instruments under nitrogen atmosphere at a heating rate of 10 ºC/min. PL emission spectra of both solution and thin-film samples were recorded on a Perkin-Elmer LS55 fluorescence spectrophotometer at 298 K. Phosphorescent spectra were determined on a Horiba Jobin Yvon Fluoromax-4 spectrometer at 77 K. The transient photoluminescence decay characteristics of the predegassed solution samples were recorded on a single photon counting controller FluoroHub-B (Horiba Jobin Yvon). The solution samples of **NA-TNA** in toluene and dimethylsulfoxide (5×10^{-6} mol/L) at room temperature were excited at 450 nm using a NanoLED-450 as the excitation light source, and the sample of **NA-TNA** in dimethylsulfoxide (5×10^{-6} mol/L) at 77 K was excited at 460 nm using a xenon flashlamp as the excitation light source, and the emitted photons were detected by a TBX detector connected to a TBX-PS power supply. Photoluminescence quantum yields (PLQYs) of the dilute solution samples were determined using Rhodamine B (75% C_2H_5OH solution, $\varphi_{PL} = 0.69$) as the standard under excitation of 460 nm; while the absolute PLQYs of the film samples were determined on a FLS 980 fluorometer (Edinburgh Instruments Ltd.) equipped with an integrating sphere and digital photometer. The UV-Vis absorption spectra were measured on a Perkin-Elmer Lambda 950 scanning spectrophotometer. The **NA-TNA**/PMMA composite thin film samples were spin-coated from their corresponding chloroform solutions with concentration of 25 mg/mL at a speed of 2000 rpm on quartz substrates; while the **NA-TNA**/CzPhONI composite thin film samples were fabricated *via* thermo-evaporation in vacuum, and the film thickness is 50 nm. The PL emission spectrum comprising both the fluorescence and phosphorescence bands of **NA-TNA** (77 K, after 2 μs delay) was deconvoluted on the basis of the assumption that both the two emission bands are Gaussian. Cyclic voltammetry (CV) measurement was carried out on a PARSTAT 2273 electrochemical workstation at room temperature in anhydrous dichloromethane solution using tetrabutylammonium perchlorate (0.1 mol/L) as the supporting electrolyte at a scanning rate of 50 mV/s. The CV system was constructed using a three-electrode electrochemical cell consisted of a Pt-wire working electrode, a Pt-wire counter electrode, and a $Ag/AgNO_3$ reference electrode (0.1 mol/L in acetonitrile) under protection of nitrogen, and each measurement was calibrated with a ferrocene/ferrocenium (Fc/Fc^+) redox system as the internal standard. Melting points were determined on a X-6 microscopic melting point apparatus.

Computational method

Quantum chemical optimizations on the energy levels of **NA-TNA** in the ground state and the lowest singlet and triplet excited states were performed using the Gaussian 09 package.[35] The ground state and the lowest triplet excited state were optimized using the density functional theory (DFT) with restricted BP86 and unrestricted BP86 (UBP86) at the basis set level of 6-31G(d,p), respectively, while the lowest singlet state geometry optimization was done by means of time dependent DFT (TDDFT) at BP86/6-31G(d,p) level. Full geometry optimizations were performed without any symmetry constraint. Also, all geometries were confirmed as stationary structures by the presence of only real frequencies at the same level of theory. Transition energies, oscillator strength and natural transition orbitals (NTOs)[36] were evaluated using TDDFT calculations at the levels of M06-2X/6-311G(d,p) for the S_0 and T_1 states, and B3LYP/6-311G(d,p) for the S_1 state, based on their corresponding opti-

mized geometries. Considering the solvent effects, all the calculations above were carried out in DMSO media within the framework of the polarized continuum model.[37,38]

OLED fabrication and measurements

Indium-tin oxide (ITO) coated glass substrates were cleaned with alcohol, acetone, and deionized water sequentially before used and then treated by oxygen plasma for 2 min. Organic functional layers were thermo-evaporated in vacuum (3×10^{-4} Pa) with a deposition rate of 2~3 Å/s, then metallic cathode was deposited with a rate of 2~3 Å/s at 3×10^{-3} Pa. The active area of the OLEDs was 1×1 mm^2. Immediately after the sample preparation, the current density-voltage-luminance (*J-V-L*) characteristics of the OLEDs were measured with a Keithley 2611 Source Meter and PR705 Spectra Colorimeter, which can also record EL spectra and Commission Internationale de l'Eclairage (CIE) coordinates accurately. All of the measurements were conducted in air at room temperature. The EQE_{max} of the OLEDs were calculated with a computer program on the basis of previous reported literature.[39]

Transient electroluminescence decay measurement

For the transient EL experiments, a pulse generator (Agilent 8114A, 100 V/2 A) was used to apply rectangular pulse voltage of 9 V to our devices. The pulse repetition rate was 500 Hz with width of 20 μs. The emission of the OLEDs was collected by an optic fiber connected to a Hamamatsu photomultiplier (PMT) (H10721–20) with the time resolution of 0.57 ns. The PMT was connected to one of the channel of a digital oscilloscope (Tektronix DPO7104, sampling rate: 5 GS/s; resolution: 100 μV) with 50 Ω input resistance. In order to extract the remnant and trapped carriers in the OLEDs (which would recombine and produce delayed fluorescence), an offset voltage of -4 V was inserted between the voltage pulses.

Magneto-electroluminescence (MEL) measurements

For the MEL measurements, the magnetic field with maximum strength of 200 mT was applied parallel to the device surface (perpendicular to the current direction). A Keithley 2612 Source Meter was used to provide the voltage bias from one channel and simultaneously recorded the current signals. Another channel of Keithley 2612 was used to record the EL intensity of the OLEDs collected by an optic fiber connected to a highly sensitive Hamamatsu photomultiplier (H10721-20). During the test, the photomultiplier was placed far away from the electromagnet to make sure there is no magnetic field dependence on its output. The resolution of MEL response has been tested to be 0.01%. In this method, the EL signals before and after the subjection to the magnetic field were recorded to calculate the average value of the zero-field signals. The magnetic field effects in EL were obtained by $MEL=\Delta EL/EL=(EL(B)-EL(aver,0))/EL(aver,0)$. All the measurements were carried out in ambient atmosphere without encapsulation.

Results and discussion

Excited-state properties of NA-TNA

To validate the ICT character of **NA-TNA**, UV-Vis absorption and PL emission spectra of **NA-TNA** in solvents with different polarity were measured (10^{-6} mol/L). As shown in Fig. 2 and Table 1, although no significant solvent effect could be observed in its absorption spectra, the PL emission spectra of **NA-TNA** display distinct positive solvatochromism. In nonpolar cyclohexane (CHX), **NA-TNA** shows a fluorescence band with vibrational structure (λ_{PLmax} = 505 nm), which could be chiefly assigned to the $^1\pi\pi^*$ transition of **NA-TNA**; with increasing solvent polarity, the emission spectrum of **NA-TNA** becomes broadened and bathochromic-shifted (e.g., λ_{PLmax} = 540 nm in Tol; λ_{PLmax} = 608 nm in THF; λ_{PLmax} = 634 nm in DCM; and λ_{PLmax} = 687 nm in DMSO), indicative of the strong ICT character of its lowest singlet excited state. Additionally, according to the Lippert-Mataga plot of **NA-TNA** (Fig. 3), a good linear correlation between solvent polarity parameter and emission maxima ($\tilde{\upsilon}_f^{max}$) could be achieved, confirming the ICT nature of its S_1 state in more polar environments.

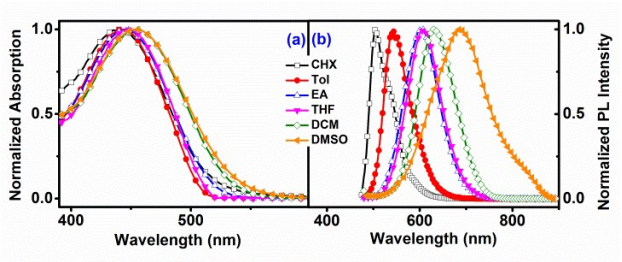

Fig. 2 (a) Normalized absorption and (b) normalized fluorescence spectra of **NA-TNA** in solvents with different polarity under excitation of 460 nm. Here, CHX denotes cyclohexane; Tol denotes toluene; EA denotes ethyl acetate; THF denotes tetrahydrofuran; DCM denotes dichloromethane; and DMSO denotes dimethylsulfoxide.

Table 1 Photophysical properties of **NA-TNA** in solvents with different polarity.

Solvent	NA-TNA				
	$f(\varepsilon)-1/2f(n^2)$	λ_{absmax} [a] (nm)	λ_{PLmax} [b] (nm)	$\tilde{\upsilon}_f^{max}$ (cm^{-1})	φ_{PL} [c]
CHX	0.110	442	505	19802	0.46
Tol	0.127	443	540	18519	0.34
EA	0.282	445	605	16529	0.28
THF	0.308	446	608	16447	0.26
DCM	0.319	453	634	15773	0.06
DMSO	0.374	455	687	14556	0.00

[a] λ_{abs}: absorption maximum; [b] λ_{em}: fluorescence maximum (λ_{ex} = 460 nm); [c] φ_{PL}: PL quantum yield.

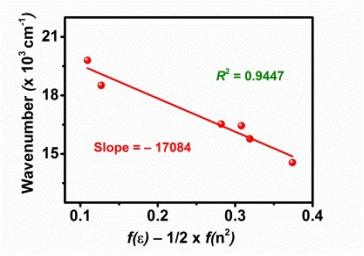

Fig. 3 Lippert-Mataga plot of the wave number of the emission maxima $\tilde{\upsilon}_f^{max}$ of **NA-TNA** versus solvent polarity parameter $f(\varepsilon\text{-}n) = f(\varepsilon) - 1/2f(n^2)$.[40]

In Tol solution, **NA-TNA** displays a biexponential decay (λ_{em} = 540 nm, τ_1 = 0.22 ns, 25.0%; τ_2 = 2.26 ns, 75.0%); while in DMSO solution, its fluorescence decay could only be well-fitted by a tri-exponential function (λ_{em} = 687 nm, τ_1 = 0.08 ns, 97.9%; τ_2 = 0.45 ns, 2.0%; τ_3 = 1.82 ns, 0.1%) (Fig. 4a and Table S1). Taking into account that **NA-TNA** shows much red-shifted emission band in DMSO (λ_{PLmax} = 687 nm), its ultra-low PLQY in DMSO (φ_{PL}~0) and much shortened lifetime could be ascribed to its much lowered energy gap that favors the non-radiative internal conversion process.[41] Nevertheless, after being cooled to 77 K, the PL intensity of **NA-TNA** was observed to increase significantly, together with drastically increased decay lifetime (λ_{em} = 620 nm, τ_1 = 0.530 μs, 62.0%; τ_2 = 1.554 μs, 24.0%; τ_3 = 6.369 μs, 14.0%) (Fig. 4b and Table S1). After being delayed for 2 μs, a newly emerged emission band at longer wavelength with λ_{PLmax} = 775 nm was observed (Fig. 5), which could be safely assigned to the phosphorescence of **NA-TNA**. It is noteworthy that with prolonged delay time of 30 μs, although the phosphorescence band disappeared, the emission band with λ_{PLmax} of 640 nm still could be observed, indicative of its delayed fluorescence (DF) feature. Taking into consideration that the concentration of **NA-TNA** is as low as 5 × 10^{-6} M, the TTA process of **NA-TNA** in this frozen sample should be inefficient, hence the DF should not be of P-type, *i.e.*, TFDF.

Accordingly, the energy levels of the $^1\pi\pi^*$ (2.55 eV) and ^{1}CT* (2.20 eV) states of **NA-TNA** were determined from the onset of its fluorescence bands in nonpolar CHX and polar DMSO, respectively;[42] while the T_1 energy level of **NA-TNA** was estimated to be 1.96 eV from the onset of its phosphorescence spectrum[42] through spectral deconvolution (Fig. S1). Consequently, the ΔE_{st} of **NA-TNA** was calculated to be 0.24 eV.

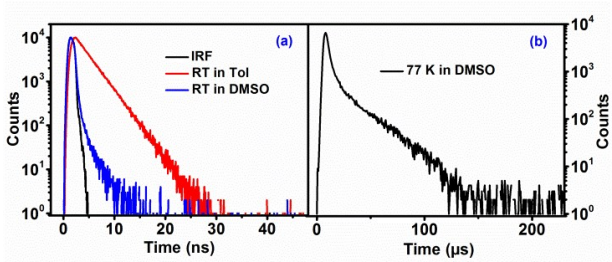

Fig. 4 (a) Fluorescence decay curves of **NA-TNA** in N_2-saturated Tol solution (monitored at 540 nm) and DMSO solution (monitored at 687 nm) at room temperature (RT) (λ_{ex} = 450 nm); and (b) the PL decay curve of **NA-TNA** in DMSO solution (monitored at 620 nm) at 77 K (λ_{ex} = 460 nm). Concentration: 5 × 10^{-6} M.

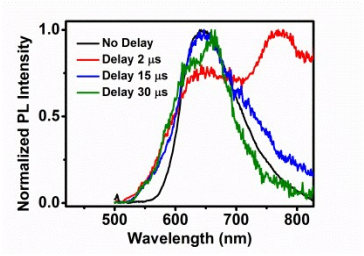

Fig. 5 Transient PL characteristics of **NA-TNA** in DMSO solution (5 × 10^{-6} M) at 77 K (λ_{ex} = 460 nm).

Theoretical calculations

To better understand the properties of the excited states of **NA-TNA**, quantum chemical calculations on the ground state, the lowest singlet and triplet excited states of **NA-TNA** were performed using the Gaussian 09 package. As depicted in Fig. 6, for the $S_0 \rightarrow S_1$ transition in the ground state of **NA-TNA**, the hole is mainly delocalized on the whole D-π-A molecular skeleton of **NA-TNA**, while the particle is mainly localized on the π-A moiety. Hence the $S_0 \rightarrow S_1$ excitation of **NA-TNA** should contain a major part of $\pi\pi^*$-featured transition with some contribution of CT transition from D to A subunits. While in the case of the lowest singlet state (S_1), the hole and particle are predominantly localized on the D-π and A moieties of **NA-TNA**, respectively, implying that the radiation process from S_1 to S_0 should be prevailed with CT character. Differed from the S_1 state, the hole and particle NTOs of the lowest triplet state were both found to be localized mainly on the π-A moiety, indicating that the radiation process of **NA-TNA** from T_1 to S_0 should be predominated with $\pi\pi^*$ character. The calculated transition energies of both the absorption and fluorescence emission bands of **NA-TNA** (2.79 eV and 1.87 eV, respectively, vide Table S2) well reproduce their corresponding experimental values (2.73 eV and 1.80 eV), suggesting that these computational results are reliable.

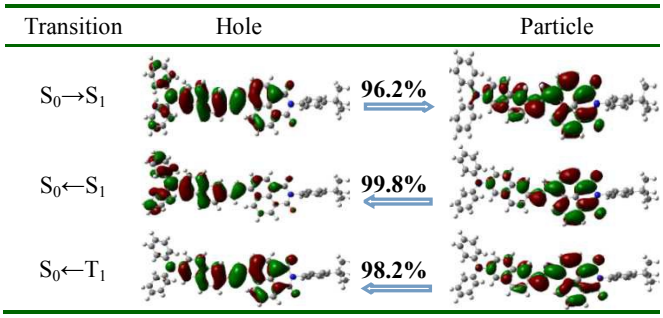

Fig. 6 The natural transition orbitals (isovalue surface 0.02 a.u.) for $S_0 \rightarrow S_1$, $S_0 \leftarrow S_1$ and $S_0 \leftarrow T_1$ transitions for **NA-TNA** in DMSO, derived from TDDFT calculations.

Consequently, according to these calculation results, the T_1 state of **NA-TNA** is of $^3\pi\pi^*$ character, while the HOMO and LUMO of **NA-TNA** in its S_1 state still have some overlap, indicative of the presence of a ^{3}CT* energy level between the $^3\pi\pi^*$ and ^{1}CT* energy levels. Because the ΔE_{ST} of **NA-TNA** is as low as 0.24 eV, the $^3\pi\pi^*$ excitons of **NA-TNA** may undergo a reverse internal conversion to its ^{3}CT* state, followed by a reverse intersystem crossing process from the ^{3}CT* state to the ^{1}CT* state.[43] Hence the DF of **NA-TNA** in DMSO solution at 77 K might be

assigned to TADF. Yet at room temperature, the T_1 state of **NA-TNA** should suffer from serious non-radiative relaxation due to the relative low bandgap of **NA-TNA**, hence no DF was observed.

Energy transfer between NA-TNA and CzPhONI

According to these photophysical and theoretical studies, **NA-TNA** should be an ICT-featured compound possessing a T_1 state with $^3\pi\pi^*$ character, hence analogous to CzPhONI,[30] **NA-TNA** may be a TFDF compound capable of utilizing triplet excitons through TTA process. However, the ultra-low PLQY of **NA-TNA** in its thin solid film state (0.068, vide **Table 2**) would limit its potential application as high-performance non-doped OLED light-emitter. As CzPhONI has been demonstrated to be a promising TFDF host material,[30] to evaluate whether CzPhONI and **NA-TNA** could act as an efficient host/guest ET pair, so that triplet excitons could be utilized concurrently by the host and guest materials in OLEDs, the absorption spectrum of **NA-TNA** and PL emission spectrum of CzPhONI in solid film states were recorded. As illustrated in Fig. 7, good spectral overlap between the emission band of CzPhONI and absorption band of **NA-TNA** could be observed, implying effective ET may take place between them. Further PL characterizations on **NA-TNA** doped PMMA films (Fig. S2) and **NA-TNA** doped CzPhONI films at different doping levels (Fig. 7) indicated that even in the 1.4 wt% **NA-TNA** doped CzPhONI film, no emission from CzPhONI could be observed, implying that the ET between **NA-TNA** and CzPhONI is quite efficient. The 1.4 wt% **NA-TNA** doped CzPhONI film displays a high PLQY of 0.802; but with increasing **NA-TNA** composition (6.0 wt%, 10.0 wt% and 15.0 wt%), the PLQY of the blending films drops gradually (0.668, 0.605, and 0.336 in sequence), which may be ascribed to the concentration quenching of **NA-TNA**. Yet even at a high doping level of 10 wt%, a satisfactory PLQY of 0.605 could be achieved, indicating that the molecular interactions in **NA-TNA** is not much serious, and high-performance heavily doped OLEDs may be achieved using **NA-TNA** as guest compound.

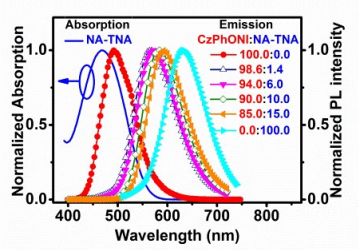

Fig. 7 Normalized fluorescence spectrum of CzPhONI, absorption spectrum of **NA-TNA**, and fluorescence spectra of **NA-TNA** in CzPhONI at different doping levels in solid film state (λ_{ex} = 380 nm).

It should be pointed out that at relatively low doping levels (≤ 10 wt%), the PLQYs of **NA-TNA** doped CzPhONI films are even higher than that of the **NA-TNA** solution (~46%), which should be an abnormal phenomenon. After careful structural analysis, we conjectured that in solution state, the presence of a diphenylamino group in **NA-TNA** may trigger intramolecular rotation that exhausts the energy of the excited states,[44] *i.e.*, **NA-TNA** might be an aggregation-induced-emission-enhancement (AIEE) luminogen. Consequently, the PL behavior of NA-TNA in CH_3CN/water mixtures with different water fraction (f_w) was investigated (Fig. S3). The results indicated that **NA-TNA** is AIEE-active in CH_3CN, hence the much enhanced PLQYs of **NA-TNA**:CzPhONI film samples may arise from the restriction of intramolecular rotation of **NA-TNA** in condensed state.

Thermal and electrochemical properties

The thermal stability of **NA-TNA** was investigated by thermogravimetric analysis (TGA) and differential scanning calorimetry (DSC) (diagrams shown in Fig. S4, S5). **NA-TNA** has a high decomposition temperature of 423 ºC (T_d corresponds to the temperature at 5 wt% loss). According to DSC measurement, although no distinct T_g could be identified, **NA-TNA** shows a high melting point of 278 ºC. Thus **NA-TNA** displays good thermostability, which is highly desirable for the OLED applications.

To estimate the energy levels of the frontier orbitals of **NA-TNA**, the electrochemical properties of **NA-TNA** has been investigated by cyclic voltammetry in degassed DCM solution (5×10^{-4} mol/L) with Fc/Fc^+ redox couple as the internal standard. As shown in Fig. S6, during the anodic scan from 0 to 0.7 V, a reversible oxidation process could be observed in **NA-TNA**, and its $E^{ox}_{1/2}$ was determined to be 0.52 V relative to Fc/Fc^+. Hence by comparison with the Fc/Fc^+ redox couple whose energy level is –4.80 eV in vacuum, the highest occupied molecular orbital (HOMO) energy level of **NA-TNA** was calculated to be –5.32 eV. As no reduction wave could be detected due to the limited range available in DCM, the lowest unoccupied molecular orbital (LUMO) energy level of –3.00 eV was deduced from the HOMO energy level and optical bandgap of **NA-TNA** according to the equation of LUMO = HOMO + E_g. As the HOMO and LUMO energy levels of CzPhONI are –5.64 eV and –3.14 eV, respectively,[30] CzPhONI could act as a suitable host for **NA-TNA**.

Electroluminescence properties

To evaluate whether **NA-TNA** is a TFDF material capable of harvesting triplet excitons *via* TTA process, firstly, we fabricated device I with **NA-TNA** as non-doped light-emitting material, and the device structure is ITO/MoO_3 (1 nm)/TCTA (40 nm)/CBP (2 nm)/**NA-TNA** (20 nm)/ TPBI (45 nm)/ LiF (1 nm)/Al (80 nm), where TCTA (4,4',4''-tri(*N*-carbazolyl)triphenylamine) acts as hole-transporting material, TPBI (1,3,5-tris(1-phenyl-1*H*-benzo[*d*]imidazol-2-yl)benzene) acts as electron-transporting material (energy level diagram shown in Fig. 8).

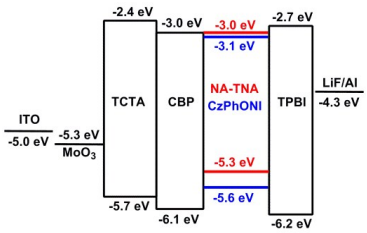

Fig. 8 Device configuration and energy level diagram of devices I, II, III, and IV.

Table 2 EL performance of devices I, II, III, and IV and PL maximum and PLQY of the corresponding active films.

Device	V_{on} (V)	L_{max} (cd/m^2)	LE_{max} [a] (cd/A)	λ_{ELmax} [b] (nm)	EQE_{max} [c]	CIE (x, y) [d]	PLQY [e]	λ_{PLmax} [f] (nm)
I	4.2	5099	0.53 (124, 5.6)	639 (6)	0.59% (124)	(0.64, 0.36) (6)	0.068	635
II	2.6	24900	3.19 (5, 3.2)	570 (10)	2.49% (5)	(0.47, 0.50) (10)	0.802	566
III	2.8	31940	7.73 (12, 3.2)	583 (10)	5.83% (12)	(0.51, 0.48) (10)	0.668	575
IV	3.2	27640	5.41 (8, 3.2)	608 (10)	4.14% (8)	(0.57, 0.43) (10)	0.336	592

[a] Data in parentheses are the corresponding EL brightness (cd/m^2) and driving voltages (V); [b] Data in parentheses are the corresponding driving voltages; [c] Data in parentheses are the corresponding EL brightness (cd/m^2); [d] Data in parentheses are the corresponding driving voltages (V); [e] PLQY data of the corresponding active films; [f] PL maximum of the corresponding active films.

The current density-voltage-luminance (*J*–*V*–*L*) and the current efficiency–current density characteristics of device I are shown in Fig. 9a and Fig. S7, respectively. The EL spectra of device I under different driving voltages are shown in Fig. S8, and some representative data are summarized in Table 2. At positive bias of 6 V, device I could emit red EL with λ_{ELmax} of 639 nm and CIE coordinates of (0.64, 0.36). The maximum brightness (L_{max}) and current efficiency (LE_{max}) of device I is 5100 cd/m^2 and 0.53 cd/A, respectively. Since the PLQY of the neat film of **NA-TNA** is as low as 0.068, the EL performance of this non-doped OLED is quite satisfactory. In fact, the EQE_{max} of device I is 0.59%, which is much higher than that predicted from the 25% singlet production limit (0.34%), indicative of the effective utilization of triplet excitons in this device. Because magneto-electroluminescence (MEL) measurement has been verified to be an effective method to identify TTA process,[45,46] here, we employed MEL measurement to testify if the triplet excitons were harvested through TTA process in device I. As shown in Fig. 9b, at low driving voltage of 4 V (around the turn-on voltage), the MEL of device I increases sharply within the low-field hyperfine regime (< 20 mT), then becomes saturated with increasing magnetic field, suggesting that there is no significant TTA process in device I. Yet with increasing applied bias hence increasing current density, the MEL of device I shows a rapid increase within the low-field regime (<20 mT) and a down trend in the high-field regime (>20 mT).[45,46] Taking into consideration that the charge injection within device I is ambipolar and balanced, this negative MEL effect could be safely assigned to TTA rather than triplet-polaron interactions (TPI).[47-49] Accordingly, the TTA process becomes more remarkable in this device at higher bias, and **NA-TNA** should be a TFDF-featured light-emitting material.

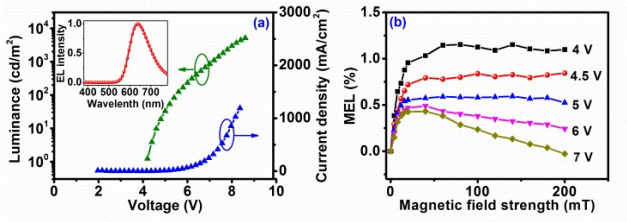

Fig. 9 (a) Current density–voltage–luminance (*J*–*V*–*L*) characteristics of device I (inset: the EL spectrum of device I at 6 V); and (b) the MEL of device I as a function of external magnetic field (MEL = $(EL(B) - EL(0))/EL(0)$).

Although the low φ_{PL} of **NA-TNA** in neat film limits its application as a non-doped OLED fluorophore, the high PLQYs of its heavily-doped films and the TFDF character of **NA-TNA** make it a quite promising guest candidate. More importantly, as **NA-TNA** and CzPhONI could form an efficient ET pair, triplet excitons could be harvested by both **NA-TNA** and CzPhONI *via* TTA process in OLEDs if heavily doped **NA-TNA**/CzPhONI films are used as the light-emissive layer. To validate this hypothesis, we fabricated two OLEDs with device configuration of ITO/MoO_3 (1 nm)/TCTA (40 nm)/CBP (2 nm)/CzPhONI:**NA-TNA** (20 nm, *x* wt%)/TPBI (45 nm)/LiF (1 nm)/Al (80 nm), where the composition of **NA-TNA** is 1.4 wt% (device II) or 6.0 wt% (device III).

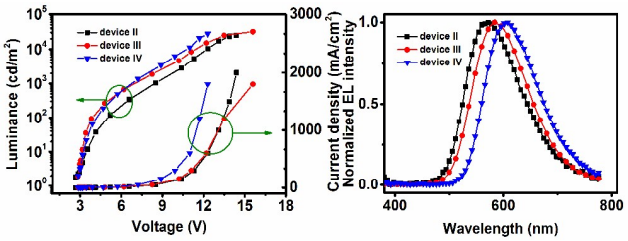

Fig. 10 (a) Current density–voltage–luminance (*J*–*V*–*L*) characteristics of devices II, III and IV; and (b) EL spectra of devices II, III and IV (at 10 V).

As shown in Fig. 10 and Table 2, at positive bias of 10 V, the 1.4 wt% **NA-TNA**-doped device II exhibits yellow emission with λ_{ELmax} of 570 nm and CIE coordinates of (0.47, 0.50), and the L_{max}, LE_{max} and EQE_{max} of this device is 24900 cd/m^2, 3.19 cd/A and 2.49%, respectively. While for device III with higher **NA-TNA** doping level of 6.0 wt%, its λ_{ELmax} is red-shifted to 583 nm with CIE coordinates of (0.51, 0.48) at 10 V, which is consistent with the PL spectral characteristics of the active layers (Fig. 7). Moreover, in comparison with that of device II, the EL performance of device III is drastically enhanced, with L_{max}, LE_{max} and EQE_{max} of 31940 cd/m^2, 7.73 cd/A and 5.83%, respectively. It is noteworthy that although the PLQY of 1.4 wt% **NA-TNA**/CzPhONI doped film is higher than that of the 6.0 wt% doped one (φ_{PL}: 0.802 *vs* 0.668), the EQE_{max} of device II is much inferior to that of the device III (2.49% *vs* 5.83%). In fact, the EQE_{max} of 5.83% has broken through the 25% singlet production limit of device III (3.34%), hence more efficient triplet exciton harvesting should occur in device III than device II.

Further MEL characterization results indicated that although analogous to device I, devices II and III also show distinct TTA-featured MEL response, they both exhibit more apparent downward trend in MEL relative to device I at higher driving voltage, and device III shows the highest TTA portion value among the three devices (Fig. 9b, Fig. 11). For the non-doped device I, the

TTA process of the **NA-TNA** triplet excitons should be a competitive process with the radiative and non-radiative decay processes. Since the relative low bandgap of **NA-TNA** would favor the non-radiative decay process, the TTA process in device I might be less efficient. For device II, as the composition of **NA-TNA** is as low as 1.4 wt%, most of the triplet excitons should be formed on CzPhONI upon charge injection, which might undergo radiative/non-radiative decay, TTA, and Dexter ET process to **NA-TNA**. Taking into consideration that the Dexter ET process should be inefficient in this low doping-level device,[50] and the higher bandgap of CzPhONI relative to **NA-TNA** should be adverse to the non-radiative decay of triplet excitons, the TTA process for CzPhONI excitons may be more efficient, hence higher TTA portion value was observed in device II than in device I. Yet it should be pointed out that the triplet excitons of **NA-TNA** formed through direct charge injection or Dexter ET in device II could not be utilized effectively due to the low composition of **NA-TNA**. In the case of device III, however, as the guest composition is as high as 6 wt%, although the triplet excitons should be formed mainly on CzPhONI upon direct charge injection, some triplet excitons could also be formed on **NA-TNA** through charge trapping or efficient Dexter ET.[51,52] Since the composition of CzPhONI is still as high as 94 wt%, similar to device II, CzPhONI should also contribute to the harvesting of triplet excitons *via* TTA process in device III; but the triplet excitons of **NA-TNA** could also be utilized *via* TTA process owing to the relatively high doping level of **NA-TNA**. Consequently, in device III, both the host and the guest compounds could contribute to the harvesting of triplet excitons, which may account for the higher TTA portion value in this device.

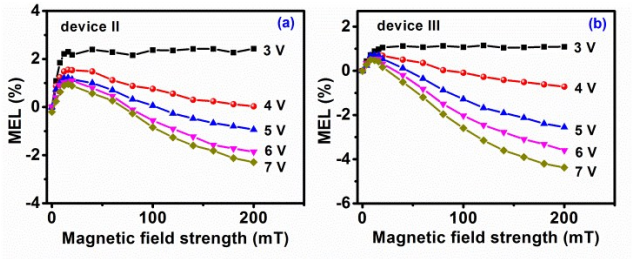

Fig. 11 The MEL of device II(a) and III(b) as a function of external magnetic field (MEL = $(EL(B) - EL(0))/EL(0)$).

To gain further insights into the origin of the high efficiency of device III, we measured the transient EL of devices I-III. As shown in Fig. 12, although all these three devices show micro-second-scaled DF, the relative DF intensity in device III is much higher than that in device I or II, confirming the more efficient TTA process in device III.

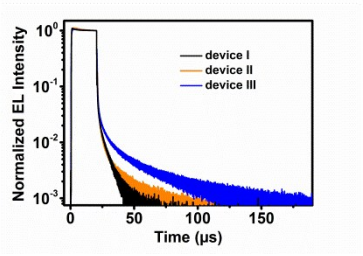

Fig. 12 Transient EL response of devices I-III (driven under rectangular pulsed voltages of 9 V with an offset of -4 V).

In principle, at higher guest doping-level, the triplet excitons of **NA-TNA** formed through Dexter ET and charge trapping processes could be utilized more efficiently *via* TTA process, yet the dropped PLQY stemming from the concentration quenching of **NA-TNA** should be adverse to the device efficiency. To confirm this conjecture, we fabricated device IV with **NA-TNA** doping-level of 15 wt%. Despite the fact that the PLQY of the active layer is as low as 0.336, device IV shows a relatively high EQE_{max} of 4.14%, note that the 25% singlet production limit of device IV should just be 1.68%. Hence the triplet exciton harvesting efficiency is indeed higher in device IV than device III. Nevertheless, the EQE_{max} of device IV is still inferior to that of device III (4.14% *vs* 5.83%), which should be attributed to the much lower PLQY of the active layer of device IV (0.336 *vs* 0.668). Therefore, to get OLEDs with high *EQE*, a trade-off between triplet exciton harvesting efficiency and concentration quenching should be achieved.

According to the energy level diagram, a possible mechanism of the TTA and ET processes within device III is tentatively proposed (Fig. 13). Upon charge injection, most of the singlet and triplet excitons are formed on CzPhONI with ^{1}CT* and ^{3}CT* character, respectively. As efficient ET could take place between CzPhONI and **NA-TNA**, most of the ^{1}CT* excitons of the host could be transformed into the ^{1}CT* excitons of **NA-TNA** through Förster ET process. But the majority of the ^{3}CT* triplets of CzPhONI would be quenched by its lower-lying $^3\pi\pi^*$ state.[30]

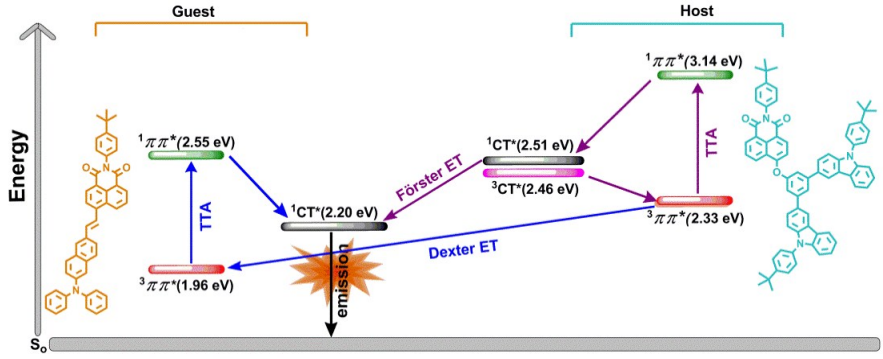

Figure 13. Schematic diagram for the proposed TTA and energy transfer processes in device III.

Taking into consideration that the concentration of **NA-TNA** in device III is 6 wt%, some $^3\pi\pi^*$ excitons of CzPhONI could be transformed into the triplet excitons of **NA-TNA** *via* Dexter ET

process,[51-52] which could be converted into $^1\pi\pi^*$ excitons of **NA-TNA** through TTA process. While the rest $^3\pi\pi^*$ excitons of CzPhONI could undergo a TTA process to generate $^1\pi\pi^*$ excitons of CzPhONI, which could be converted to ^{1}CT* *via* internal conversion. Consequently, in device III with relatively high guest concentration, the triplet excitons could be effectively harvested not only by the host compound, but also by the guest compound, resulting in high EL performance.

Conclusions

A red naphthalimide derivative with D-π-A molecular structure, namely **NA-TNA** was designed and synthesized. Photophysical characterization revealed that **NA-TNA** is an ICT-featured compound; while theoretical calculation and MEL characterization indicated that **NA-TNA** is a promising TFDF material because its lowest triplet energy level possesses $^3\pi\pi^*$ character. In addition, **NA-TNA** could form an efficient ET pair with the TFDF-charactered host compound CzPhONI due to their structural similarity, and the presence of a bulky diphenylamine D subunit in **NA-TNA** endows it with suppressed intermolecular interactions, thereupon high PLQY could be achieved in **NA-TNA**/CzPhONI blending films at relatively high guest doping levels. Taking advantages of the TFDF characters of both **NA-TNA** and CzPhONI and the relatively high PLQY of the heavily-doped guest/host active-layer, in OLED with 6 wt% doped **NA-TNA**/CzPhONI film as the emissive layer, triplet excitons could be harvested efficiently not only by the host, but also by the guest materials through TTA process, hence the device displays high performance with L_{max} of 31940 cd/m^2 and LE_{max} of 7.73 cd/A, and the EQE_{max} is 5.83%, which breaks through the 25% singlet production limit of this device. Our results indicated that ICT-featured TFDF compounds should be quite promising OLED light-emitting materials, and may shed light on the molecular design strategy for the guest fluorophores to achieve high-performance OLEDs by way of TFDF.

Notes and references

[a] *Key Laboratory of Green Chemistry and Technology (Ministry of Education), College of Chemistry, Sichuan University, Chengdu 610064, P. R. China. E-mail: luzhiyun@scu.edu.cn;*
[b] *State Key Laboratory of Supramolecular Structure and Materials, Jilin University, Changchun 130012, P. R. China. E-mail:lifeng01@jlu.edu.cn;*
[c] *State Key Laboratory of Luminescence and Applications, Changchun Institute of Optics, Fine Mechanics and Physics, Chinese Academy of Sciences, Changchun 130033, P. R. China. E-mail: liuxy@ciomp.ac.cn;*
[d] *College of Chemistry and Materials Science, Sichuan Normal University, Chengdu 610068, P. R. China.*

† Electronic Supplementary Information (ESI) available: synthetic procedures and characterization data, photophysical and elecrochemical properties, electroluminescence properties, ^{1}NMR, ^{13}C NMR, FT-IR, and HRMS spectra. See DOI: 10.1039/b000000x/

‡ These authors contributed equally.

Acknowledgements

We acknowledge the financial support for this work by National Natural Science Foundation of China (Projects 21190031, 61275036, 21372168, U1230121, and 21432005), and CAS Innovation Program. We are grateful to the Analytical & Testing Center of Sichuan University and Comprehensive Training Platform of Specialized Laboratory, College of Chemistry, Sichuan University for providing NMR data for the intermediates and objective molecules.

References

1 C. W. Tang and S. A. VanSlyke, *Appl. Phys. Lett.*, 1987, **51**, 913–915.
2 M. A. Baldo, D. F. O'Brien, Y. You, A. Shoustikov, S. Sibley, M. E. Thompson and S. R. Forrest, *Nature*, 1998, **395**, 151–154.
3 Y. Tao, K. Yuan, T. Chen, P. Xu, H. H. Li, R. F. Chen, C. Zheng, L. Zhang and W. Huang, *Adv. Mater.*, 2014, **26**, 7931–7958.
4 L. Yao, B. Yang and Y. G. Ma, *Sci. China: Chem.*, 2014, **57**, 335–345.
5 M. Segal, M. A. Baldo, R. J. Holmes, S. R. Forrest and Z. G. Soos, *Phys. Rev. B: Condens. Matter Mater. Phys.*, 2003, **68**, 075211.
6 L. Xiao, Z. Chen, B. Qu, J. Luo, S. Kong, Q. Gong and J. Kido, *Adv Mater.*, 2011, **23**, 926–952.
7 K. Goushi, K. Yoshida, K. Sato and C. Adachi, *Nat. Photonics.*, 2012, **6**, 253–258.
8 A. P. Monkman, *ISRN Mater. Sci.*, 2013, **2013**, 670130.
9 Y. Im and J. Y. Lee, *Chem. Mater.*, 2014, **26**, 1413−1419.
10 T. Komino, H. Nomura, T. Koyanagi and C. Adachi, *Chem. Mater.*, 2013, **25**, 3038–3047.
11 H. Uoyama,K.Goushi, K. Shizu, H. Nomura and C. Adachi, *Nature,* 2012, **492**, 234−238.
12 W. J. Li, Y. Y. Pan, R. Xiao, Q. M. Peng, S. T. Zhang, D. G. Ma, F. Li, F. Z. Shen, Y. H. Wang, B. Yang and Y. G. Ma, *Adv. Funct. Mater.*, 2014, **24**, 1609−1614.
13 L. Yao, S. T. Zhang, R. Wang, W. J. Li, F. Z. Shen, B. Yang and Y. G. Ma, *Angew. Chem.*, 2014, **126**, 2151–2155.
14 W. J. Li, Y. Y. Pan, L. Yao, H. C. Liu, S. T. Zhang, C. Wang, F. Z. Shen, P. Lu, B. Yang and Y. G. Ma, *Adv. Opt. Mater.*, 2014, **2**, 892−901.
15 D. Fan, Y. P. Yi, Z. D. Li, W. J. Liu, Q. Peng and Z. G. Shuai, *J. Phys. Chem. A*, 2014, DOI: 10.1021/jp5099409.
16 Y. Zhang and S. R. Forrest, *Phys. Rev. Lett.*, 2012, **108**, 267404/1−267404/5.
17 C.-J. Chiang, A. Kimyonok, M. K. Etherington, G. C. Griffiths, V. Jankus, F. Turksoy and A. P. Monkman, *Adv. Funct. Mater.*, 2013, **23**, 739–746.
18 V. Jankus, C.-J. Chiang, F. Dias and A. P. Monkman, *Adv. Mater.*, 2013, **25**, 1455–1459.
19 Y. C. Luo and H. Aziz, *Adv. Funct. Mater.*, 2010, **20**, 1285–1293.
20 S. M. King, M. Cass, M. Pintani, C. Coward, F. B. Dias, A. P. Monkman and M. Roberts, *J. Appl. Phys.*, 2011, **109**, 074502/1−074502/5.
21 D. Yokoyama, Y. Park, B. Kim, S. Kim, Y. J. Pu, J. Kido and J. Park, *Appl. Phys. Lett.*, 2011, **99**, 123303/1–123303/3.
22 S. K. Kim, B. Yang, Y. G. Ma, J. H. Lee and J. W. Park, *J. Mater. Chem.*, 2008, **18**, 3376–3384.
23 P. Y. Chou, H. H. Chou, Y. H. Chen, T. H. Su, C. Y. Liao, H. W. Lin, W. C. Lin, H. Y. Yen, I. C. Chen and C. H. Cheng, *Chem. Commun.*, 2014, **50**, 6869–6871.
24 H. Fukagawa, T. Shimizu, N. Ohbe, S. Tokito, K. Tokumaru and H. Fujikake, *Org. Electron.*, 2012, **13**, 1197–1203.
25 J. Mezyk, R. Tubino, A. Monguzzi, A. Mech and F. Meinardi, *Phys. Rev. Lett.*, 2009, **102**, 087404/1−087404/4.
26 Y. L. Lei, Y. Zhang, R. Liu, P. Chen, Q. L. Song and Z. H. Xiong, *Org. Electron.*, 2009, **10**, 889–894.
27 Y. Zhang, R. Liu, Y. L. Lei and Z. H. Xiong, *Appl. Phys. Lett.*, 2009, **94**, 083307/1−083307/3.
28 A. Ryasnyanskiy and I. Biaggio, *Phys. Rev. B: Condens. Matter Mater. Phys.*, 2011, **84**, 193203/1−193203/4.
29 P. Irkhin and I. Biaggio, *Phys. Rev. Lett.*, 2011, **107**, 017402/1−017402/4.
30 J. Zhou, P. Chen, X. Wang, Y. Wang, Y. Wang, F. Li, M. H. Yang, Y. Huang, J. S. Yu and Z. Y. Lu, *Chem. Commun.*, 2014, **50**, 7586–7589.
31 J. Li, D. Liu, Z. Hong, S. Tong, P. Wang, C. Ma, O. Lengyel, C.-S.

Lee, H.-L. Kwong and S. Lee, *Chem. Mater*., 2003, **15**, 1486–1490.
32 J. Massin, W. Dayoub, C. Mulatier, C. Aronica, Y. Bretonnière and C. Andraud, *Chem. Mater*., 2011, **23**, 862–873.
33 M. L. Jia, X. N. Ma, L. Y. Yan, H. F. Wang, Q. J. Guo, X. F. Wang, Y. Y. Wang, X. W. Zhan and A. D. Xia, *J. Phys. Chem. A*, 2010, **114**, 7345−7352.
34 Y. Wang, J. Zhou, X. Wang, X. J. Zheng, Z. Y. Lu, W. Zhang, Y. Q. Chen, Y. Huang, X. M. Pu and J. S. Yu, *Dyes Pigm*., 2014, **100**, 87–96.
35 M. J. Frisch, G. W. Trucks, H. B. Schlegel, Gaussian 09, Revision A.02; Gaussian, Inc, Wallingford CT, 2009.
36 R. L. Martin, *J. Chem. Phys.,* 2003, **118**, 4775−4777.
37 M. Cossi, G. Scalmani, N. Rega and V. Barone, *J. Chem. Phys*., 2002, **117**, 43–54.
38 V. Barone, M. Cossi and J. Tomasi, *J. Chem. Phys.*, 1997, **107**, 3210–3221.
39 S. Okamoto, K. Tanka, Y. Izumi, H. Adachi, T. Yamaji and T. Suzuki, *Jpn. J. Appl. Phys*., 2001, **40**, 783–784.
40 K. A. Zachariasse, S. I. Druzhinin, W. Bosch and R. Machinek, *J. Am. Chem. Soc*., 2004, **126**, 1705−1715.
41 Y. S. Yao, J. Xiao, X. S. Wang, Z. B. Deng and B. W. Zhang, *Adv. Funct. Mater*., 2006, **16**, 709 –718.
42 F. B. Dias, K. N. Bourdakos, V. Jankus, K. C. Moss, K. T. Kamtekar, V. Bhalla, J. Santos, M. R. Bryce and A. P. Monkman, *Adv. Mater.*, 2013, **25**, 3707–3714.
43 Q. Zhang, J. Li, K. Shizu, S. Huang, S. Hirata, H. Miyazaki and C. Adachi, *J. Am. Chem. Soc*., 2012, **134**, 14706−14709.
44 Y. Hong, J. W. Y. Lam and B. Z. Tang, *Chem. Soc. Rev.*, 2011, **40**, 5361−5388.
45 P. Chen, Z. Xiong, Q. Peng, J. Bai, S. Zhang and F. Li, *Adv. Opt. Mater*., 2014, **2**, 142–148.
46 M. Shao, L. Yan, M. Li, I. Ilia and B. Hu, *J. Mater. Chem. C*, 2013, **1**, 1330 –1336.
47 R. C. Johnson, R. E. Merrifield, P. Avakian, and R. B. Flippen, *Phys. Rev. Lett*., 1967, **19**, 285.
48 R. Liu, Y. Zhang, Y. L. Lei, P. Chen and Z. H. Xiong, *J. Appl. Phys*., 2009, **105**, 093719/1−093719/5.
49 B. Hu and Y. Wu, *Nat. Mater*., 2007, **6**, 985–991.
50 M. A. Wolak, J. Delcamp, C. A. Landis, P. A. Lane, J. Anthony and Z. Kafafi, *Adv. Funct. Mater*., 2006, **16**, 1943–1949.
51 D. Wasserberg, S. C. J. Meskers and R. A. J. Janssen, *J. Phys. Chem. A*, 2007, **111**, 1381–1388.
52 H. Fukagawa, T. Shimizu, H. Hanashima, Y. Osada, M. Suzuki and H. Fujikake, *Adv. Mater*., 2012, **24**, 5099−5103.

Table of contents

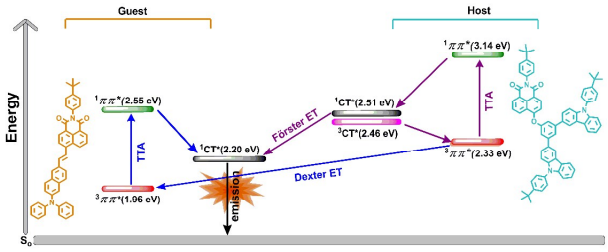

Triplet excitons could be harvested simultaneously by both guest and host materials with intramolecular charge-transfer feature *via* triplet-triplet annihilation in heavily–doped OLED.